A STUDY OF HYPERSPECTRAL CLUSTERING – HOW TO SPEED UP SPECTRAL UNMIXING OF MOON MINERALOGY MAPPER DATA

M. Arnaut, K. Wohlfarth, C. Wöhler, Image Analysis Group TU Dortmund University, Germany
{mirza.arnaut,kay.wohlfarth,christian.woehler}@tu-dortmund.de

Introduction: Hyperspectral images are the key to remote mineral analysis of planetary surfaces. These images are usually acquired in the infrared region in which unique mineral absorp-tion bands are present. These bands can be used to derive spectral features, which help to identify and to map minerals on the target body (e.g. [1]). More rigorous physical approaches enable spectral unmixing [2], which additionally allows to quantitatively infer abundance maps of minerals. Spectral unmixing is a rich field of research with many laboratory studies (e.g., [3, 4, 5]) or studies on the target bodies (e.g., [6, 7]).

Due to the high spatial and spectral resolution of many hyperspectral sensors, pixelwise spectral unmix-ing of large regions become computationally demanding. To handle large datasets, a viable preprocessing step is to cluster similar spectra into distinct regions. Each of these regions [7] can subsequently be represented by only one spectrum which is used for further analysis and unmixing. This step will dramatically save processing time while the trade-off between accuracy and speed can be controlled by the number of clusters.

This investigation contributes in two ways: At first, two state-of-the-art algorithms for clustering, i.e., Gaussian-Mixture-Models (GMM) [8] and Self-Orga-nizing-Maps (SOM) [9] are applied to spectra acquired by the Moon Mineralogy Mapper (M^3) [10] to form regions of similar spectra. Secondly, we use the clustering results to apply our spectral unmixing framework [5] and construct mineral abundance maps.

Methods: We use a normalized nearly global M^3 spectral reflectance mosaic with a spatial resolution of 2 pixels per degree, which was constructed using the M^3 level 1B spectral radiance data [https://pds-imaging.jpl.nasa.gov/volumes/m3.html] using the framework described in [11,12]. Our approach takes four steps. Step 1: Up to seven spectral parameters [13] are extracted from the M^3-spectra which form a multi-dimensional feature space. After continuum removal based on the convex hull [14], the absorption wavelength (wavelength with the strongest absorp-tion), the band depth and width, and integrated band depth are determined for the absorption bands near 1 µm and 2 µm.

Step 2: An additional normalization step is applied to these parameters to ensure that they equally contribute to the feature space. Therefore, the covariance matrix Σ of the features is transformed into the unit matrix I. This is achieved by a transformation defined as $T(x) = \Omega V^T(x-\mu)$, where μ is the mean of each parameter, V is the matrix of eigenvectors and Ω is defined as $\Omega=\Lambda^{-½}$, where Λ is the diagonalized eigenvalue matrix of Σ [15]. This results in a rotation of the data, such that the eigenvectors are aligned with the coordinate axes and the scaled (matrix Ω) so they have the unit length, treating each feature equally.

Step 3: We use two approaches to perform clustering of similar spectral regions.

Gaussian-Mixture Models (GMM) [8] are probability density functions which consist of a weighted sum of parameterized Gaussian component densities. The parameters are determined by training with the expectation-maximization algorithm [8].

Self-Organizing Maps (SOM) [9] are neural networks trained in an unsupervised way. They are used to transform high-dimensional data such as hyperspectral images to a low-dimensional space effectively reducing the dimensionality. For the layer topology, we choose a random approach and set the distance between the neurons as the link distance.

One challenge of these algorithms is to determine the number of meaningful clusters. Here, we study the behavior of the results in dependence on the clusters K and trade-off between robustness and over-clustering.

Step 4: Lunar regolith is an intimate mixture which means that the reflectance spectra of the constituting minerals mix non linearly. As a solution, in [3,5] the Hapke model [16] is inverted to obtain the single scattering albedo which mixes linearly. We adopted this approach, take the spectra which form the cluster centers from Step 3 and perform spectral unmixing with respect to the Lunar Soil Characterization Consortium (LSCC) data base [17,18]. Given the detailed modal abundance analyses of the LSCC-endmembers provided by [12,13], they can be converted to mineral abundances.

Results and Conclusion: We applied GMM and SOM with different values of *K* and set K=64 which is a viable trade-off between run-time and sufficient segmentation. Larger values for *K* increase the level of detail at the expense of run-time and clustering robustness. The clustering results of the GMM and the SOM are shown in the top row of Figure 1 and 2, respectively. Figure 1 and 2 (second to fourth row) display selected mineral abundance maps of the Moon (plagioclase, total abundance of pyroxenes, olivine) for GMM and SOM, respectively. The mineral maps are largely consistent with previous studies e.g. [7,19]. The striking advantage is that we can combine spectral unmixing with the accurate laboratory analyses of the LSCC-samples in [17,18].

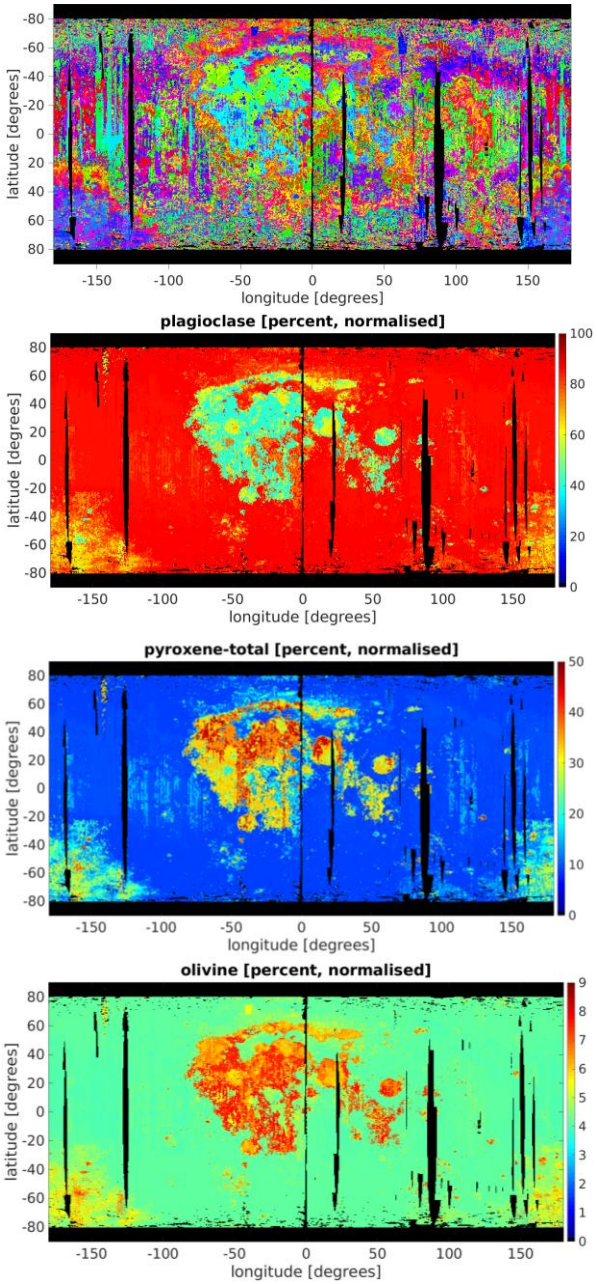

Figure 1. First row: Clustering result GMM. Colors indicate different spectral clusters. Second to fourth row: Mineral abundance maps based on the clustering.

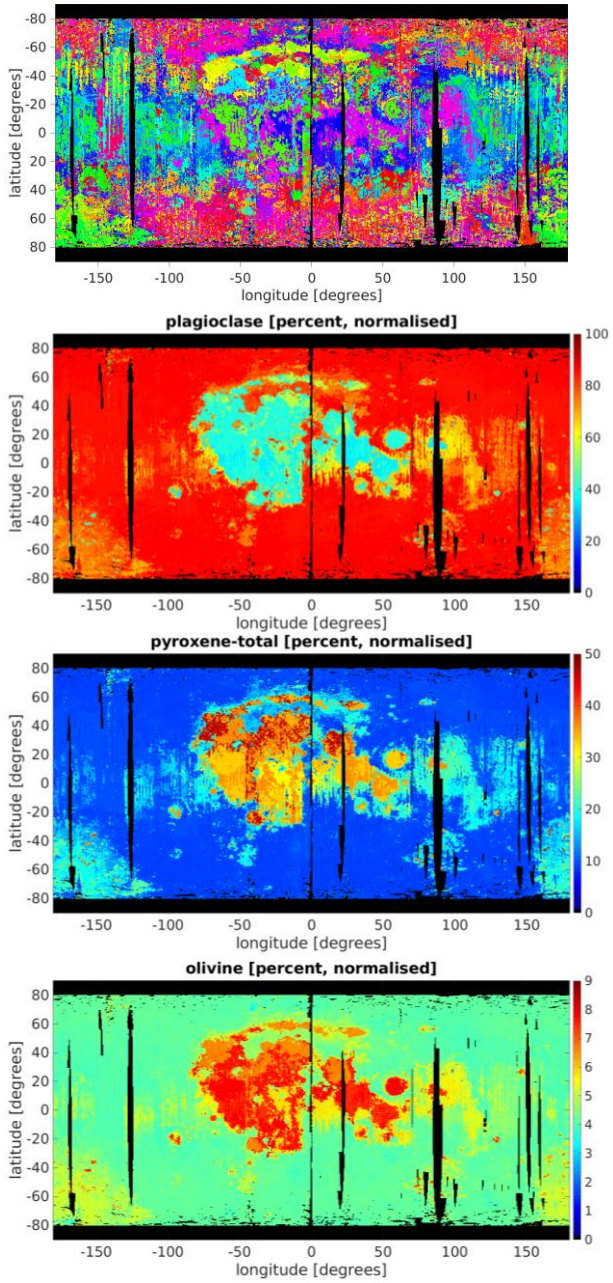

Figure 2. First row: Clustering result SOM. Colors indicate different spectral clusters. Second to fourth row: Mineral abundance maps based on the clustering.

References: [1] Sunschine, J. and Pieters, C. (1998), JGR Planets, 103, (E6), 13675-13688. [2] Keshava, N. and Mustard, J. (2002), IEEE SPM, 19, 1, 44-57. [3] Mustard, J. and Pieters, C. (1989), JGR Solid Earth, 94, (B10),13619-13634. [4] Ramsey, M.S. and Christensen, P.R. (1998), JGR., 103, 577–596. [5] Rommel, D. et al. (2017), Icarus, 284, 126-149. [6] Liu, Y. et al. (2016), JGR Planets, 121, (10), 2004-2036. [7] Bernhardt, V. et al. (2017), Int. Arch. Photogramm. Remote Sens. Spatial Inf. Sci., XLII-3/W1, 7-14. [8] Reynolds, D. (2009) in Li, S.Z. and Jain, A. (eds) Encyclopedia of Biometrics. Springer, Boston, USA. [9] Kohonen, T. (2001). Self-Organizing Maps, 3rd edn. Springer.

[10] Green, R. O. et. al (2011) JGR Planets, 116, E00G19. [11] Grumpe, A. et al. (2014), ASR 53(12), 1735-1767. [12] Wöhler, C. et al. (2017), Sci. Adv., 3, (9). [13] Mall, U. (2014) Advances in Space Research, 54, (10), 2029-2040. [14] Fu, Z. et al. (2007), *IEEE Transactions on Geoscience and Remote Sensing*, 45, (11), 3827–3844. [15] De Maesschalck, R. et al. (2000), Chemometrics and Intelligent Labrotary Systems, 50, 1, 1-18. [16] Hapke, B. (2012) Cambridge Univ. Press, Cambridge. [17] Taylor, L.A. et al., (2001), *JGRS*, 106 (E11), 27,985-28,000. [18] Taylor, L.A. et al. (2010), JGR Planets, 115, (E2). [19] Lemelin, B. et al. (2016) LPSC XXXXVII, abstract #2994.